

Article

Boundary Effect and Critical Temperature of Two-Band Superconducting FeSe Films

Chenxiao Ye ¹, Jiantao Che ² and Hai Huang ^{2,*}¹ School of Nuclear Science and Engineering, North China Electric Power University, Beijing 102206, China² Department of Mathematics and Physics, North China Electric Power University, Beijing 102206, China

* Correspondence: huanghai@ncepu.edu.cn

Abstract: Based on two-band Bogoliubov–de Gennes theory, we study the boundary effect of an interface between a two-gap superconductor FeSe and insulator (or vacuum). New boundary terms are introduced into two-band Ginzburg–Landau formalism, which modifies the boundary conditions for the corresponding order parameters of superconductor. The theory allows for a mean-field calculation of the critical temperature suppression with the decrease in FeSe film thickness. Our numerical results are in good agreement with the experimental data observed in this material.

Keywords: two-band superconductor; boundary term; critical temperature; FeSe film

1. Introduction

The discovery of iron-based materials with a high superconducting transition temperature has triggered great interest for both fundamental studies and practical applications in this field [1]. Among these superconductors, the FeSe system has a simple crystal structure, clean superconducting phase and low toxicity, making it an appealing candidate for studying the superconducting properties of Fe-based compounds [2]. The FeSe layers consist of square lattices of Fe atoms with tetrahedrally coordinated covalent bonds to the Se anions, and the lattice constant perpendicular to the layered plane is about 0.55 nm [3]. The Fermi surface of this compound consists of one electron and one-hole thin cylinders through Shubnikov–de Haas oscillations [4]. At around 100 K, FeSe shows a structural phase transition from tetragonal to orthorhombic without an accompanying magnetic phase transition and becomes superconducting below 8 K [2,5–7]. The picture of two-gap superconductivity has been clearly confirmed by the scanning tunneling microscopy measurements, multiple Andreev reflection spectroscopy, specific heat measurements and other experiments [8–12].

High-quality, superconducting thin films have an important role in applications and basic research of superconductivity. In this respect, preparing high-quality thin-film samples not only satisfies the demands for some measurements of basic physical properties but also provides suitable bases for making tunneling junctions, which determines several important superconducting parameters, such as gap value and pairing symmetry [13]. Previous studies examining the thickness dependence of FeSe have been limited to measurements on thin films grown using techniques such as molecular beam epitaxy [14,15], pulsed laser deposition [16] and radio-frequency sputtering [17], all of which require well-optimised growth protocols. An alternative to the growth of thin films is to create devices by mechanical exfoliation of high-quality single crystals. With this method, a series of FeSe superconducting films with thicknesses ranging from 470 to 2.2 nm was obtained on the Si/SiO₂ substrate [18]. A dramatic depression of T_c has been observed when the thickness is smaller than 27 nm. Farrar et al. have also observed similar behavior: a sharp decrease in superconductivity occurs at $d < 25$ nm [19]. One possible origin for this T_c suppression could be the increase in disorder scattering with reducing thickness [19,20]. Another alternative possibility is due to the interaction between FeSe thin film and the



Citation: Ye, C.; Che, J.; Huang, H. Boundary Effect and Critical Temperature of Two-Band Superconducting FeSe Films. *Crystals* **2023**, *13*, 18. <https://doi.org/10.3390/cryst13010018>

Academic Editor: Jacek Ćwik

Received: 2 December 2022

Revised: 18 December 2022

Accepted: 18 December 2022

Published: 22 December 2022



Copyright: © 2022 by the authors. Licensee MDPI, Basel, Switzerland. This article is an open access article distributed under the terms and conditions of the Creative Commons Attribution (CC BY) license (<https://creativecommons.org/licenses/by/4.0/>).

substrate [21]. However, up to now, there is still no consensus on the explanation of the experimental data mentioned above.

In this paper, we propose that the T_c dependence on the film thickness is due to the influence of the boundary effect between the two-band superconductor and the insulator (or vacuum). We first introduce the appropriate boundary conditions for the Ginzburg–Landau (GL) order parameters at the superconductor–insulator interface. We then give a microscopic analysis of these new boundary terms based on two-band Bogoliubov–de Gennes theory. Our theoretical result is consistent with the experimental data of FeSe films, which suggests the boundary effect is an important factor for the understanding of superconducting properties in this iron-based compound.

The rest of this article is structured as follows. In Section 2, we first review two-band Bogoliubov–de Gennes theory and GL equations, and then give a microscopic derivation of proper boundary conditions for the superconductor–insulator interface. In Section 3, we perform the calculations on the film-thickness-dependence of critical temperature for the FeSe compound in the context of GL theory. Finally, we conclude this article in Section 4.

2. Theoretical Scheme

Based on the previous literature [22–31], we can write the Hamiltonian of a two-band superconductor as

$$H = \sum_{i\sigma} c_{i\sigma}^\dagger(\mathbf{r}) \hat{h}(\mathbf{r}) c_{i\sigma}(\mathbf{r}) - \sum_{ii'} g_{ii'} c_{i'\uparrow}^\dagger(\mathbf{r}) c_{i\downarrow}^\dagger(\mathbf{r}) c_{i'\downarrow}(\mathbf{r}) c_{i\uparrow}(\mathbf{r}), \quad (1)$$

where $i, i' = 1, 2$ are the band indices and $\sigma = \uparrow, \downarrow$ is the spin index. $\hat{h}(\mathbf{r})$ is the single-particle Hamiltonian of the normal metal, and $g_{ii'}$ are the electron–phonon interaction constants with $g_{12} = g_{21}$.

We can introduce the gap functions as

$$\Psi_i(\mathbf{r}) = - \sum_{i'} g_{ii'} \langle c_{i'\downarrow}(\mathbf{r}) c_{i'\uparrow}(\mathbf{r}) \rangle \quad (2)$$

and transform the Hamiltonian into the mean-field form

$$H_{eff} = \sum_{i\sigma} c_{i\sigma}^\dagger(\mathbf{r}) \hat{h}(\mathbf{r}) c_{i\sigma}(\mathbf{r}) + \sum_i [\Psi_i(\mathbf{r}) c_{i\uparrow}^\dagger(\mathbf{r}) c_{i\downarrow}^\dagger(\mathbf{r}) + \text{H.c.}]. \quad (3)$$

This effective Hamiltonian can be diagonalized by means of the Bogoliubov transformation with b and b^\dagger as the annihilation and creation operators of quasi-particle excitations:

$$c_{i\uparrow}(\mathbf{r}) = \sum_{\mathbf{k}} [u_{ik}(\mathbf{r}) b_{ik\uparrow} - v_{ik}^*(\mathbf{r}) b_{ik\downarrow}^\dagger] \quad (4)$$

and

$$c_{i\downarrow}(\mathbf{r}) = \sum_{\mathbf{k}} [u_{ik}(\mathbf{r}) b_{ik\downarrow} + v_{ik}^*(\mathbf{r}) b_{ik\uparrow}^\dagger] \quad (5)$$

where \mathbf{k} is the wave vector. As a result, the effective Hamiltonian can be written as

$$H_{eff} = E_g + \sum_{ik\sigma} E_{ik} b_{ik\sigma}^\dagger b_{ik\sigma}. \quad (6)$$

E_g is the ground state energy, and E_{ik} is the energy of the excitation.

Using the commutator $[c_{i\sigma}(\mathbf{r}), H_{eff}]$, together with Equations (4)–(6), we can obtain the Bogoliubov–de Gennes equations for a two-band superconductor [32–35]

$$\begin{pmatrix} \hat{h} & \Psi_i(\mathbf{r}) \\ \Psi_i^*(\mathbf{r}) & -\hat{h}^* \end{pmatrix} \begin{pmatrix} u_{ik}(\mathbf{r}) \\ v_{ik}(\mathbf{r}) \end{pmatrix} = E_{ik} \begin{pmatrix} u_{ik}(\mathbf{r}) \\ v_{ik}(\mathbf{r}) \end{pmatrix}. \quad (7)$$

From Equation (6), we can also obtain $\langle b_{ik\uparrow}^\dagger b_{ik\uparrow} \rangle = f(E_{ik})$ with $f(E_{ik}) = [1 + \exp(E_{ik}/k_B T)]^{-1}$. Then, with Equation (2), we can transform the self-consistent gap equations into

$$\Psi_i(\mathbf{r}) = \sum_{i'k} g_{ii'} v_{i'k}^*(\mathbf{r}) u_{i'k}(\mathbf{r}) \times [1 - 2f(E_{i'k})]. \quad (8)$$

In analogy with the single-band case [36], for small gap functions Ψ_i , we can obtain the linearized form of self-consistency conditions from Equations (7) and (8) as

$$\Psi_i(\mathbf{r}) = \sum_{i'} \int K_{ii'}(\mathbf{r}, \mathbf{r}') \Psi_{i'}(\mathbf{r}') d\mathbf{r}' \quad (9)$$

with the kernel

$$K_{ii'}(\mathbf{r}, \mathbf{r}') = g_{ii'} k_B T \sum_{kk'} \frac{\Phi_{i'k}^*(\mathbf{r}') \Phi_{i'k'}^*(\mathbf{r}') \Phi_{i'k}(\mathbf{r}) \Phi_{i'k'}(\mathbf{r})}{(\varepsilon_{i'k} - i\hbar\omega)(\varepsilon_{i'k'} + i\hbar\omega)}. \quad (10)$$

$\Phi_{i'k}(\mathbf{r})$ is defined as the normal-state eigenfunction of the electron; $\hbar\Phi_{i'k} = \varepsilon_{i'k} \Phi_{i'k}$. The frequency $\omega = (2\nu + 1)\pi k_B T/\hbar$, where ν is an integer.

With the explicit expressions of the kernels in the bulk system and the addition of nonlinear terms to the gap equations, we can obtain the two-band GL equations from Equation (9) as [27]

$$\alpha_1(T) \Psi_1 + \beta_1 |\Psi_1|^2 \Psi_1 - \gamma_1 \nabla^2 \Psi_1 - \varepsilon_{12} \Psi_2 = 0 \quad (11)$$

and

$$\alpha_2(T) \Psi_2 + \beta_2 |\Psi_2|^2 \Psi_2 - \gamma_2 \nabla^2 \Psi_2 - \varepsilon_{12} \Psi_1 = 0 \quad (12)$$

with the GL parameters

$$\alpha_{1,2} = N_{1,2} \left[\frac{\lambda_{22,11}}{\lambda} - \frac{1}{\lambda_{\max}} - \ln\left(\frac{T_{c0}}{T}\right) \right], \quad \beta_i = \frac{7\zeta(3)N_i}{16\pi^2(k_B T_{c0})^2}, \quad (13)$$

$$\gamma_i = \frac{7\zeta(3)\hbar^2 N_i v_{Fi}^2}{16\pi^2(k_B T_{c0})^2} \quad \text{and} \quad \varepsilon_{12} = \frac{N_1 \lambda_{12}}{\lambda} = \frac{N_2 \lambda_{21}}{\lambda}. \quad (14)$$

$\lambda_{ii'} = g_{ii'} N_{i'}$ with $N_{i'}$ being the density of states at the Fermi level for each band; $\lambda = \lambda_{11}\lambda_{22} - \lambda_{12}\lambda_{21}$ and $\lambda_{\max} = \frac{1}{2}[(\lambda_{11} + \lambda_{22}) + \sqrt{(\lambda_{11} - \lambda_{22})^2 + 4\lambda_{12}\lambda_{21}}]$ are the determinant and the largest eigenvalue of λ -matrix, respectively. T_{c0} is the bulk critical temperature, and v_{Fi} is the average Fermi velocity for each band.

In the spatially homogeneous case, we can neglect the gradient γ -terms. Equations (11) and (12) will yield the gap equations at $T = T_{c0}$:

$$\begin{pmatrix} \lambda_{11} & \lambda_{12} \\ \lambda_{21} & \lambda_{22} \end{pmatrix} \begin{pmatrix} \Psi_1 \\ \Psi_2 \end{pmatrix} = \lambda_{\max} \begin{pmatrix} \Psi_1 \\ \Psi_2 \end{pmatrix}, \quad (15)$$

which obviously give a consistent result.

Meanwhile, we can write down the boundary conditions for the two-band GL theory at the interface between the two-band superconductor and insulator (or vacuum) as

$$\nabla \Psi_i \cdot \mathbf{s}|_S = - \sum_{i'} A_{ii'} \Psi_{i'} \quad (16)$$

with S , the boundary coordinate, and $A_{ii'}$, as some constants. From Equation (16), we can see that the ordinary Neumann boundary condition corresponds to $A_{ii'} = 0$. However, we will show that the boundary effect induced by these A -terms is important for the understanding of the T_c suppression in FeSe thin films.

At this stage, we would also like to point out the boundary effect and different interband interactions in multi-band superconductors have already been extensively studied in the literature. Babaev et al. presented a microscopic study on the behavior of the order parameters for two-band superconductors based on the free boundary condition [37]. With the Neumann boundary condition, the stable edge states and the dynamic response of such states to an external applied current have been investigated in the time-dependent Ginzburg–Landau formalism for the two-band mesoscopic superconductors [38]. Aguirre et al. also discussed the effects of different interband interactions on the vortex states by solving the two-band Ginzburg–Landau equations with the Neumann boundary condition [39,40]. However, to explain the suppression of critical temperature with the decrease in film thickness, we need to conduct detailed microscopic analysis and derive the correct boundary terms based on the two-band Bogoliubov–de Gennes theory for the superconductor FeSe.

Now, we try to derive these boundary A -terms in Equation (16) from the two-band Bogoliubov–de Gennes theory. In all cases, we assume that there is no current flowing through the boundary. The equation to be solved reads

$$\Psi_i(s) = \sum_{i'} \int K_{ii'}(s, s') \Psi_{i'}(s') ds' \quad (17)$$

where s measures the normal distance from the boundary. For simplicity, we set the cross-section of the boundary as 1. $K_{ii'}(s, s')$ is defined by Equation (10), and due to the existence of interface $\Psi_i(s)$ will decrease exponentially in the insulating regime.

Following the procedure suggested by de Gennes [36], we suppose that the form of gap functions close to the surface behaves as

$$\Psi_i(s) = \Psi_{i0} + \left(\sum_{i'} A_{ii'} \Psi_{i'0} \right) s \quad (18)$$

with Ψ_{i0} being the gap function at the boundary and $s > 0$ inside the superconductor. It is easy to see that the boundary condition in Equation (16) follows naturally from Equation (18). However, beyond the scale of the coherence length from the boundary, the linear dependence definitely becomes invalid. Ψ_i will then have a negative curvature and reach the BCS value deep in the superconductor.

If we introduce $K_{ii'}^0(s, s')$ as the kernel of gap functions in the bulk metal, we can then transform Equation (17) as

$$\begin{aligned} \Psi_i(s) - \sum_{i'} \int K_{ii'}^0(s, s') \Psi_{i'}(s') ds' \\ = - \sum_{i'} \int [K_{ii'}^0(s, s') - K_{ii'}(s, s')] \Psi_{i'}(s') ds' \equiv - \sum_{i'} H_{ii'}(s). \end{aligned} \quad (19)$$

From Equations (11) and (12) with the higher order β -terms omitted, while also noting that $K_{ii'}^0(s, s') = K_{ii'}^0(s - s')$ due to the translational symmetry, we can read out the Laplace transformation of $K_{ii'}^0$ close to the critical temperature as

$$K_{ii'}^0(p) = \frac{\lambda_{ii'}}{\lambda_{\max}} + \frac{\lambda_{ii'} \gamma_{i'}}{N_{i'}} p^2. \quad (20)$$

By plugging Equation (20) into Equation (19), we can get

$$\Psi_i(p) - \sum_{i'} (\lambda_{ii'} / \lambda_{\max}) \Psi_{i'}(p) - \sum_{i'} (\lambda_{ii'} \gamma_{i'} / N_{i'}) p^2 \Psi_{i'}(p) = - \sum_{i'} H_{ii'}(p). \quad (21)$$

$\Psi_i(p)$ and $H_{ii'}(p)$ are the Laplace transformations of $\Psi_i(s)$ and $H_{ii'}(s)$, respectively. Since the first two terms of the left-handed side in Equation (21) can be approximately canceled out according to Equation (15), we have

$$\sum_{i'} (\lambda_{ii'} \gamma_{i'} / N_{i'}) p^2 \Psi_{i'}(p) = \sum_{i'} H_{ii'}(p). \quad (22)$$

We can see that both sides in Equation (22) take the main contribution from the boundary region. Notice that the Laplace transformation of the gap functions in Equation (18) takes the form

$$\Psi_i(p) = \frac{\Psi_{i0}}{p} + \sum_{i'} \frac{A_{ii'} \Psi_{i'0}}{p^2}. \quad (23)$$

Then, at $p \rightarrow 0$, we will obtain from Equation (22)

$$\sum_{i'i''} (\lambda_{ii'} \gamma_{i'} / N_{i'}) A_{i'i''} \Psi_{i''0} = \sum_{i'} H_{ii'}(p=0). \quad (24)$$

According to de Gennes' analysis [36,41], from the sum rules

$$\int K_{ii'}^0(s, s') ds' = \frac{\lambda_{ii'}}{\lambda_{\max}} \quad \text{and} \quad \int K_{ii'}(s, s') ds' = \frac{\lambda_{ii'} N_{i'}(s)}{\lambda_{\max} N_{i'}} \quad (25)$$

with $N_{i'}(s)$ as the local density of states at the Fermi surface, we can write the Laplace transformation of the kernel difference at $p \rightarrow 0$ as

$$H_{ii'}(p=0) = \int H_{ii'}(s) ds = \frac{\lambda_{ii'} \Psi_{i'0}}{\lambda_{\max}} \int \frac{\Psi_{i'}(s)}{\Psi_{i'0}} \left[1 - \frac{N_{i'}(s)}{N_{i'}} \right] ds. \quad (26)$$

$\Psi_{i'}(s)/\Psi_{i'0}$ approaches zero in the insulating region, and is of the order of one in the metallic region. $N_{i'}(s)/N_{i'}$ also passes from $0 \rightarrow 1$ a few atoms from the boundary. Therefore, the integrand in Equation (26) is nonvanishing only in a width of the order of the lattice constant a . We can then estimate $H_{ii'}(p=0)$ as

$$H_{ii'}(p=0) = \frac{\lambda_{ii'} a}{\lambda_{\max}} \Psi_{i'0}. \quad (27)$$

By combining Equation (24) with Equation (27), we can finally obtain

$$A_{ii} = \frac{N_i a}{\gamma_i \lambda_{\max}} \quad \text{and} \quad A_{12} = A_{21} = 0. \quad (28)$$

With these formulae, we successfully demonstrate the microscopic origin of boundary conditions in Equation (16).

Based on two-band GL theory, we can write the supercurrent at the boundary S as

$$J_S = -ie\hbar \sum_{i=1}^2 \frac{1}{m_i} [\Psi_i^* (\nabla \Psi_i \cdot \mathbf{s})|_S - \Psi_i (\nabla \Psi_i^* \cdot \mathbf{s})|_S]. \quad (29)$$

According to our boundary conditions, we have the supercurrent

$$J_S = -\frac{ie\hbar}{m_1} [\Psi_1^* (-A_{11} \Psi_1) - \Psi_1 (-A_{11} \Psi_1^*)] - \frac{ie\hbar}{m_2} [\Psi_2^* (-A_{22} \Psi_2) - \Psi_2 (-A_{22} \Psi_2^*)] = 0, \quad (30)$$

which definitely gives a consistent result.

3. Critical Temperature of FeSe Films in Ginzburg–Landau Theory

In this section, we try to understand the film-thickness-dependence of T_c for FeSe based on the boundary effect mentioned above. We suppose that the film extends from $z = -d/2$ to $z = d/2$ and the film thickness is d .

From Equations (11) and (12), two-band GL equations can be written as

$$\begin{pmatrix} \hat{H}_{11} & \hat{H}_{12} \\ \hat{H}_{21} & \hat{H}_{22} \end{pmatrix} \begin{pmatrix} \Psi_1(\mathbf{r}) \\ \Psi_2(\mathbf{r}) \end{pmatrix} = 0 \quad (31)$$

with

$$\hat{H}_{ii} = -\gamma_i \nabla^2 + \alpha_i(T) \quad (32)$$

and

$$\hat{H}_{12} = \hat{H}_{21} = -\epsilon_{12}. \quad (33)$$

Note that close to the critical temperature, the magnitudes of order parameters are small, and the higher order β -terms can be neglected.

Similarly to the single-band case [41], we set the form of gap functions for the superconducting film as

$$\begin{pmatrix} \Psi_1(z) \\ \Psi_2(z) \end{pmatrix} = \begin{pmatrix} \eta_1 \cos(k_1 z) \\ \eta_2 \cos(k_2 z) \end{pmatrix} \quad (34)$$

with η_i as the constant. Then, from the boundary conditions

$$\left. \frac{d\Psi_i}{dz} \right|_{z=\pm d/2} = \mp A_{ii} \Psi_i, \quad (35)$$

we have k_i , satisfying

$$k_i \tan\left(\frac{k_i d}{2}\right) = A_{ii}. \quad (36)$$

Let us introduce

$$H_{ii'} = \langle \Psi_i | \hat{H}_{ii'} | \Psi_{i'} \rangle = \int_{-d/2}^{d/2} \Psi_i(z) \hat{H}_{ii'} \Psi_{i'}(z) dz. \quad (37)$$

We can transform Equation (31) into

$$\begin{pmatrix} H_{11} & H_{12} \\ H_{21} & H_{22} \end{pmatrix} \begin{pmatrix} \eta_1 \\ \eta_2 \end{pmatrix} = 0 \quad (38)$$

with

$$H_{ii} = \left[\gamma_i k_i^2 + \alpha_i(T) \right] \left[\frac{d}{2} + \frac{\sin(k_i d)}{2k_i} \right] \quad (39)$$

and

$$H_{12} = H_{21} = -\epsilon_{12} \left[\frac{\sin(\frac{k_1 d}{2} + \frac{k_2 d}{2})}{k_1 + k_2} + \frac{\sin(\frac{k_1 d}{2} - \frac{k_2 d}{2})}{k_1 - k_2} \right]. \quad (40)$$

The critical temperature of the two-band superconducting film will be determined by the condition

$$H_{11} H_{22} - H_{12} H_{21} = 0 \quad (41)$$

at $T = T_c$, which can be explicitly written as

$$\prod_{i=1,2} \left[\gamma_i k_i^2 + \alpha_i(T_c) \right] \left[\frac{d}{2} + \frac{\sin(k_i d)}{2k_i} \right] = \epsilon_{12}^2 \left[\frac{\sin(\frac{k_1 d}{2} + \frac{k_2 d}{2})}{k_1 + k_2} + \frac{\sin(\frac{k_1 d}{2} - \frac{k_2 d}{2})}{k_1 - k_2} \right]^2. \quad (42)$$

For the two-band superconductor FeSe, we have $T_{c0} \approx 8$ K [5] and the average lattice constant $a \approx 0.55$ nm [3]. The density of states at the Fermi level for each band are $N_1 = 0.30$ and $N_2 = 0.65$ eV⁻¹, respectively, [8,42]. From the numerical work in reference [43], we can get $\lambda_{11} = g_{11}N_1 = 0.30$ and the ratio $g_{11}:g_{12}:g_{22} = 1:0.30:0.37$. Then, we have $\lambda = 0.054$, $\lambda_{\max} = 0.41$ and $\epsilon_{12} = 1.1$ eV⁻¹. With the average Fermi velocities $v_{F1} = 3.7$ and $v_{F2} = 4.4$ in units of 10^{13} nm · s⁻¹ [44], we get $\gamma_1 = 20$ nm² · eV⁻¹ and $\gamma_2 = 61$ nm² · eV⁻¹ from Equation (14). Then, from Equation (28), we can obtain the characteristic length scales $A_{11} = (50 \text{ nm})^{-1}$ and $A_{22} = (70 \text{ nm})^{-1}$. For a given film thickness d , we first get k_i from Equation (36). By plugging it into Equation (42), the critical temperature T_c as a function of d can be calculated numerically and then plotted in Figure 1. It is shown that the critical temperature keeps gradually decreasing with the decreases in d and $T_c \approx 3$ K when the film thickness is reduced to $d = 3$ nm. From Figure 1, we can see that our theoretical results fit the experimental data on Si/SiO₂ substrate well.

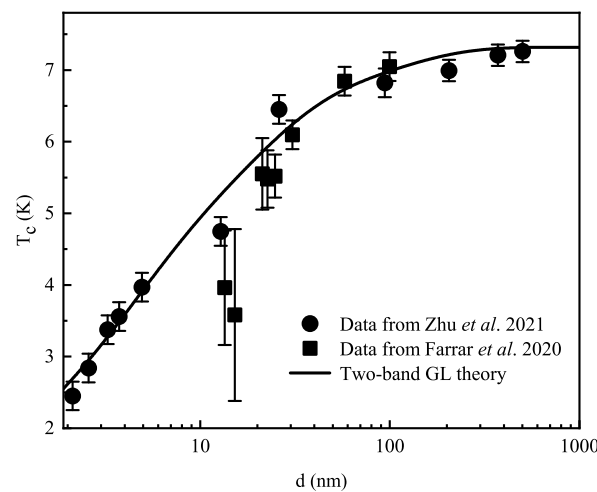


Figure 1. The critical temperature as a function of FeSe film thickness. The experimental data are taken from Ref. [18] (circles) and Ref. [19] (squares) respectively.

At this point, we can also discuss the single-band superconducting system of niobium [45,46], which shows similar behavior to FeSe. The critical temperature of Nb films gradually decreases with a reduction in the thickness from 300 to about 50 nm. A much stronger dependence of the critical temperature on thickness is observed for films thinner than 50 nm. We would also like to apply our theoretical scheme with the similar boundary condition $\nabla\Psi \cdot s|_S = -A\Psi$ to understand this physical property for single-band superconductor Nb. With the lattice constant $a = 0.33$ nm, the Fermi velocity $v_F = 3.9$ in units of 10^{13} nm · s⁻¹, the density of states at the Fermi level $N = 1.5$ eV⁻¹ and the dimensionless interaction parameter $\lambda = 0.32$ for niobium [47,48], we can obtain $\gamma = \frac{7\zeta(3)\hbar^2 N v_F^2}{16\pi^2 (k_B T_{c0})^2} = 80$ nm² · eV⁻¹ with the bulk critical temperature $T_{c0} = 9.4$ K and $A = \frac{Na}{\gamma\lambda} = (52 \text{ nm})^{-1}$. Thus, with this characteristic length scale, our theoretical scenario can qualitatively explain the strong T_c suppression around 50 nm in the single-band superconducting Nb films.

4. Conclusions

In conclusion, we introduced the appropriate boundary conditions in two-band GL theory at the interface between two-gap superconductor and insulator (or vacuum). We also gave a microscopic derivation of these boundary terms based on two-band Bogoliubov–de Gennes formalism. For the two-band superconductor FeSe, we obtained the characteristic length scales of the boundary effect as 50 and 70 nm. The theory can perfectly explain the dramatic suppression of T_c when the film thickness is reduced to the same order of these

length scales. Our investigation thus suggests that the boundary effect induced by these new terms may play an important role in the research of some iron-based superconducting films.

Author Contributions: Conceptualization, C.Y., J.C. and H.H.; methodology, C.Y., J.C. and H.H.; software, C.Y.; validation, C.Y., J.C. and H.H.; formal analysis, C.Y., J.C. and H.H.; investigation, C.Y., J.C. and H.H.; resources, H.H.; data curation, C.Y., J.C. and H.H.; writing—original draft preparation, C.Y.; writing—review and editing, C.Y., J.C. and H.H.; visualization, C.Y.; supervision, J.C. and H.H.; project administration, H.H. All authors have read and agreed to the published version of the manuscript.

Funding: This research received no external funding.

Data Availability Statement: Not applicable.

Conflicts of Interest: The authors declare no conflict of interest.

References

1. Kamihara, Y.; Watanabe, T.; Hirano, M.; Hosono, H. Iron-Based layered superconductor $\text{La}[\text{O}_{1-x}\text{F}_x]\text{FeAs}$ ($x=0.05-0.12$) with $T_c = 26$ K. *J. Am. Chem. Soc.* **2008**, *130*, 3296–3297. [[CrossRef](#)] [[PubMed](#)]
2. Hsu, F.C.; Luo, J.Y.; Yeh, K.W.; Chen, T.K.; Huang, T.W.; Wu, P.M.; Lee, Y.C.; Huang, Y.L.; Chu, Y.Y.; Yan, D.C.; et al. Superconductivity in the PbO-type structure α -FeSe. *Proc. Natl. Acad. Sci. USA* **2008**, *105*, 14262. [[CrossRef](#)] [[PubMed](#)]
3. Schneider, R.; Zaitsev, A.G.; Fuchs, D.; Löhneysen, H.V. Excess conductivity and Berezinskii-Kosterlitz-Thouless transition in superconducting FeSe thin films. *J. Phys. Condens. Matter* **2014**, *26*, 455701. [[CrossRef](#)] [[PubMed](#)]
4. Terashima, T.; Kikugawa, N.; Kiswandhi, A.; Choi, E.S.; Brooks, J.S.; Kasahara, S.; Watashige, T.; Ikeda, H.; Shibauchi, T.; Matsuda, Y.; et al. Anomalous Fermi surface in FeSe seen by Shubnikov-de Haas oscillation measurements. *Phys. Rev. B* **2014**, *90*, 144517. [[CrossRef](#)]
5. McQueen, T.M.; Williams, A.J.; Stephens, P.W.; Tao, J.; Zhu, Y.; Ksenofontov, V.; Casper, F.; Felser, C.; Cava, R.J. Tetragonal-to-orthorhombic structural phase transition at 90 K in the superconductor $\text{Fe}_{1.01}\text{Se}$. *Phys. Rev. Lett.* **2009**, *103*, 057002. [[CrossRef](#)]
6. McQueen, T.M.; Huang, Q.; Ksenofontov, V.; Felser, C.; Xu, Q.; Zandbergen, H.; Hor, Y.S.; Allred, J.; Williams, A.J.; Qu, D.; et al. Extreme sensitivity of superconductivity to stoichiometry in $\text{Fe}_{1+\delta}\text{Se}$. *Phys. Rev. B* **2009**, *79*, 014522. [[CrossRef](#)]
7. Watson, M.D.; Kim, T.K.; Haghighirad, A.A.; Davies, N.R.; McCollam, A.; Narayanan, A.; Blake, S.F.; Chen, Y.L.; Ghannadzadeh, S.; Schofield, A.J.; et al. Emergence of the nematic electronic state in FeSe. *Phys. Rev. B* **2015**, *91*, 155106. [[CrossRef](#)]
8. Wang, Q.Y.; Li, Z.; Zhang, W.H.; Zhang, Z.C.; Zhang, J.S.; Li, W.; Ding, H.; Ou, Y.B.; Deng, P.; Chang, K.; et al. Interface-induced high-temperature superconductivity in single unit-cell FeSe films on SrTiO_3 . *Chin. Phys. Lett.* **2012**, *29*, 037402. [[CrossRef](#)]
9. Chareev, D.; Osadchii, E.; Kuzmicheva, T.; Lin, J.Y.; Kuzmichev, S.; Volkova, O.; Vasiliev, A. Single crystal growth and characterization of tetragonal FeSe_{1-x} superconductors. *Cryst. Eng. Commun.* **2013**, *15*, 1989. [[CrossRef](#)]
10. Lin, J.Y.; Hsieh, Y.S.; Chareev, D.A.; Vasiliev, A.N.; Parsons, Y.; Yang, H.D. Coexistence of isotropic and extended s-wave order parameters in FeSe as revealed by low-temperature specific heat. *Phys. Rev. B* **2011**, *84*, 220507(R). [[CrossRef](#)]
11. Schneider, R.; Zaitsev, A.G.; Fuchs, D.; Hott, R. Anisotropic field dependence of the electronic transport in superconducting FeSe thin films. *Supercond. Sci. Technol.* **2020**, *33*, 075011. [[CrossRef](#)]
12. Sun, Y.; Zhang, W.H.; Xing, Y.; Li, F.S.; Zhao, Y.F.; Xia, Z.C.; Wang, L.L.; Ma, X.C.; Xue, Q.K.; Wang, J. High temperature superconducting FeSe films on SrTiO_3 substrates. *Sci. Rep.* **2014**, *4*, 6040. [[CrossRef](#)] [[PubMed](#)]
13. Chen, T.K.; Luo, J.Y.; Ke, C.T.; Chang, H.H.; Huang, T.W.; Yeh, K.W.; Chang, C.C.; Hsu, P.C.; Wu, C.T.; Wang, M.J.; et al. Low-temperature fabrication of superconducting FeSe thin films by pulsed laser deposition. *Thin Solid Films* **2010**, *519*, 1540. [[CrossRef](#)]
14. Tan, S.Y.; Zhang, Y.; Xia, M.; Ye, Z.Y.; Chen, F.; Xie, X.; Peng, R.; Xu, D.F.; Fan, Q.; Xu, H.C.; et al. Interface-induced superconductivity and strain-dependent spin density waves in FeSe/ SrTiO_3 thin films. *Nat. Mater.* **2013**, *12*, 634. [[CrossRef](#)] [[PubMed](#)]
15. Wang, Q.Y.; Zhang, W.H.; Zhang, Z.C.; Sun, Y.; Xing, Y.; Wang, Y.Y.; Wang, L.L.; Ma, X.C.; Xue, Q.K.; Wang, J. Thickness dependence of superconductivity and superconductor-insulator transition in ultrathin FeSe films on SrTiO_3 (001) substrate. *2D Mater.* **2015**, *2*, 044012. [[CrossRef](#)]
16. Nabeshima, F.; Imai, Y.; Hanawa, M.; Tsukada, I.; Maeda, A. Enhancement of the superconducting transition temperature in FeSe epitaxial thin films by anisotropic compression. *Appl. Phys. Lett.* **2013**, *103*, 172602. [[CrossRef](#)]
17. Schneider, R.; Zaitsev, A.G.; Fuchs, D.; Löhneysen, H.V. Superconductor-insulator quantum phase transition in disordered FeSe thin films. *Phys. Rev. Lett.* **2012**, *108*, 257003. [[CrossRef](#)]
18. Zhu, C.S.; Lei, B.; Sun, Z.L.; Cui, J.H.; Shi, M.Z.; Zhuo, W.Z.; Luo, X.G.; Chen, X.H. Evolution of transport properties in FeSe thin flakes with thickness approaching the two-dimensional limit. *Phys. Rev. B* **2021**, *104*, 024509. [[CrossRef](#)]
19. Farrar, L.S.; Bristow, M.; Haghighirad, A.A.; McCollam, A.; Bending, S.J.; Coldea, A.I. Suppression of superconductivity and enhanced critical field anisotropy in thin flakes of FeSe. *NPJ Quantum Mater.* **2020**, *5*, 29. [[CrossRef](#)]

20. Böhmer, A.E.; Taufour, V.; Straszheim, W.E.; Wolf, T.; Canfield, P.C. Variation of transition temperatures and residual resistivity ratio in vapor-grown FeSe. *Phys. Rev. B* **2016**, *94*, 024526.
21. Phan, G.N.; Nakayama, K.; Sugawara, K.; Sato, T.; Urata, T.; Tanabe, Y.; Tanigaki, K.; Nabeshima, F.; Imai, Y.; Maeda, A.; et al. Effects of strain on the electronic structure, superconductivity, and nematicity in FeSe studied by angle-resolved photoemission spectroscopy. *Phys. Rev. B* **2017**, *95*, 224507. [[CrossRef](#)]
22. Suhl, H.; Matthias, B.T.; Walker, L.R. Bardeen-Cooper-Schrieffer theory of superconductivity in the case of overlapping bands. *Phys. Rev. Lett.* **1959**, *3*, 552–554. [[CrossRef](#)]
23. Moskalenko, V.A. Superconductivity in metals with overlapping energy bands. *Fiz. Metal. Metalloved* **1959**, *8*, 2518–2520.
24. Tilley, D.R. The Ginzburg-Landau equations for pure two band superconductors. *Proc. Phys. Soc.* **1964**, *84*, 573. [[CrossRef](#)]
25. Tilley, D.R. The Ginzburg-Landau equations for anisotropic alloys. *Proc. Phys. Soc.* **1965**, *86*, 289. [[CrossRef](#)]
26. Gurevich, A. Enhancement of the upper critical field by nonmagnetic impurities in dirty two-gap superconductors. *Phys. Rev. B* **2003**, *67*, 184515. [[CrossRef](#)]
27. Zhitomirsky, M.E.; Dao, V.H. Ginzburg-Landau theory of vortices in a multigap superconductor. *Phys. Rev. B* **2004**, *69*, 054508. [[CrossRef](#)]
28. Dao, V.H.; Zhitomirsky, M.E. Anisotropy of the upper critical field in MgB₂: The two-gap Ginzburg-Landau theory. *Eur. Phys. J. B* **2005**, *44*, 183. [[CrossRef](#)]
29. Gurevich, A. Limits of the upper critical field in dirty two-gap superconductors. *Physica C* **2007**, *456*, 160. [[CrossRef](#)]
30. Silaev, M.; Babaev, E. Microscopic theory of type-1.5 superconductivity in multiband systems. *Phys. Rev. B* **2011**, *84*, 094515. [[CrossRef](#)]
31. Silaev, M.; Babaev, E. Microscopic derivation of two-component Ginzburg-Landau model and conditions of its applicability in two-band systems. *Phys. Rev. B* **2012**, *85*, 134514. [[CrossRef](#)]
32. Zhang, L.F.; Covaci, L.; Milošević, M.V.; Berdiyrov, G.R.; Peeters, F.M. Unconventional vortex states in nanoscale superconductors due to shape-induced resonances in the inhomogeneous cooper-pair condensate. *Phys. Rev. Lett.* **2012**, *109*, 107001. [[CrossRef](#)] [[PubMed](#)]
33. Zhang, L.F.; Covaci, L.; Milošević, M.V.; Berdiyrov, G.R.; Peeters, F.M. Vortex states in nanoscale superconducting squares: The influence of quantum confinement. *Phys. Rev. B* **2013**, *88*, 144501. [[CrossRef](#)]
34. Zhang, L.F.; Becerra, V.F.; Covaci, L.; Milošević, M.V. Electronic properties of emergent topological defects in chiral *p*-wave superconductivity. *Phys. Rev. B* **2016**, *94*, 024520. [[CrossRef](#)]
35. Zhang, L.F.; Covaci, L.; Milošević, M.V. Topological phase transitions in small mesoscopic chiral *p*-wave superconductors. *Phys. Rev. B* **2017**, *96*, 224512. [[CrossRef](#)]
36. de Gennes, P.G. *Superconductivity of Metals and Alloys*; Westview Press: New York, NY, USA, 1966.
37. Benfenati, A.; Samoilenka, A.; Babaev, E. Boundary effects in two-band superconductors. *Phys. Rev. B* **2021**, *103*, 144512. [[CrossRef](#)]
38. Gonçalves, W.C.; Sardella, E.; Becerra, V.F.; Milošević, M.V.; Peeters, F.M. Numerical solution of the time dependent Ginzburg-Landau equations for mixed (*d*+*s*)-wave superconductors. *J. Math. Phys.* **2014**, *55*, 041501. [[CrossRef](#)]
39. Aguirre, C.; Martins, Q.D.; Barba-Ortega, J. Vortices in a superconducting two-band disk: Role of the Josephson and bi-quadratic coupling. *Physica C* **2021**, *581*, 1353818. [[CrossRef](#)]
40. Aguirre, C.; de Arruda, A.; Faúndez, J.; Barba-Ortega, J. ZFC process in 2+1 and 3+1 multi-band superconductor. *Physica B* **2021**, *615*, 413032. [[CrossRef](#)]
41. Ketterson, J.B.; Song, S.N. *Superconductivity*; Cambridge University Press: Cambridge, UK, 1999.
42. Subedi, A.; Zhang, L.J.; Singh, D.J.; Du, M.H. Density functional study of FeS, FeSe, and FeTe: Electronic structure, magnetism, phonons, and superconductivity. *Phys. Rev. B* **2008**, *78*, 134514. [[CrossRef](#)]
43. Chen, Y.J.; Zhu, H.P.; Shanenko, A.A. Interplay of Fermi velocities and healing lengths in two-band superconductors. *Phys. Rev. B* **2020**, *101*, 214510. [[CrossRef](#)]
44. Tamai, A.; Ganin, A.Y.; Rozbicki, E.; Bacsá, J.; Meevasana, W.; King, P.D.C.; Caffio, M.; Schaub, R.; Margadonna, S.; Prassides, K.; et al. Strong electron correlations in the normal state of the iron-based FeSe_{0.42}Te_{0.58} superconductor observed by angle-resolved photoemission spectroscopy. *Phys. Rev. Lett.* **2010**, *104*, 097002. [[CrossRef](#)] [[PubMed](#)]
45. Ilin, K.S.; Vitusevich, S.A.; Jin, B.B.; Gubin, A.I.; Klein, N.; Siegel, M. Peculiarities of the thickness dependence of the superconducting properties of thin Nb films. *Physica C* **2004**, *408–410*, 700. [[CrossRef](#)]
46. Gubin, A.I.; Ilin, K.S.; Vitusevich, S.A.; Siegel, M.; Klein, N. Dependence of magnetic penetration depth on the thickness of superconducting Nb thin films. *Phys. Rev. B* **2005**, *72*, 064503. [[CrossRef](#)]
47. Chen, L.Z.; Wang, X.C.; Wen, Y.H.; Zhu, Z.Z. Jahn-Teller effect in Nb planar atomic sheet. *Acta Phys. Sin.* **2007**, *56*, 2920. [[CrossRef](#)]
48. Li, C.Z.; Li, C.; Wang, L.X.; Wang, S.; Liao, Z.M.; Brinkman, A.; Yu, D.P. Bulk and surface states carried supercurrent in ballistic Nb-Dirac semimetal Cd₃As₂ nanowire-Nb junctions. *Phys. Rev. B* **2018**, *97*, 115446. [[CrossRef](#)]

Disclaimer/Publisher's Note: The statements, opinions and data contained in all publications are solely those of the individual author(s) and contributor(s) and not of MDPI and/or the editor(s). MDPI and/or the editor(s) disclaim responsibility for any injury to people or property resulting from any ideas, methods, instructions or products referred to in the content.